Biosensors and Bioelectronics 97 (2017) 107–114

Contents lists available at ScienceDirect

Biosensors and Bioelectronics

journal homepage: www.elsevier.com/locate/bios

Highly sensitive photoelectrochemical biosensor for kinase activity detection and inhibition based on the surface defect recognition and multiple signal amplification of metal-organic frameworks

Zonghua Wang[b,*], Zhiyong Yan[a,b,d], Feng Wang[a], Jibao Cai[c,*], Lei Guo[c], Jiakun Su[c], Yang Liu[a,*]

[a] Department of Chemistry, Beijing Key Laboratory for Analytical Methods and Instrumentation, Key Lab of Bioorganic Phosphorus Chemistry and Chemical Biology (Ministry of Education), Tsinghua University, Beijing 100084, China
[b] Shandong Sino-Japanese Center for Collaborative Research of Carbon Nanomaterials, Collaborative Innovation Center for Marine Biomass Fiber Materials and Textiles, College of Chemistry and Chemical Engineering, Laboratory of Fiber Materials and Modern Textile, The Growing Base for State Key Laboratory, Qingdao University, Shandong 266071, China
[c] Center of R & D, China Tobacco Jiangxi Industrial Co. Ltd., Nanchang 330096, China
[d] Beijing Center for Physical and Chemical Analysis, Beijing 100089, China

ARTICLE INFO

Keywords:
Kinase
Metal-organic frameworks
Surface defect recognition
Signal amplification
Photoelectrochemical biosensor

ABSTRACT

A turn-on photoelectrochemical (PEC) biosensor based on the surface defect recognition and multiple signal amplification of metal-organic frameworks (MOFs) was proposed for highly sensitive protein kinase activity analysis and inhibitor evaluation. In this strategy, based on the phosphorylation reaction in the presence of protein kinase A (PKA), the Zr-based metal-organic frameworks (UiO-66) accommodated with $[Ru(bpy)_3]^{2+}$ photoactive dyes in the pores were linked to the phosphorylated kemptide modified TiO_2/ITO electrode through the chelation between the Zr^{4+} defects on the surface of UiO-66 and the phosphate groups in kemptide. Under visible light irradiation, the excited electrons from $[Ru(bpy)_3]^{2+}$ adsorbed in the pores of UiO-66 injected into the TiO_2 conduction band to generate photocurrent, which could be utilized for protein kinase activities detection. The large surface area and high porosities of UiO-66 facilitated a large number of $[Ru(bpy)_3]^{2+}$ that increased the photocurrent significantly, and afforded a highly sensitive PEC analysis of kinase activity. The detection limit of the as-proposed PEC biosensor was 0.0049 U mL^{-1} (S/N!=!3). The biosensor was also applied for quantitative kinase inhibitor evaluation and PKA activities detection in MCF-7 cell lysates. The developed visible-light PEC biosensor provides a simple detection procedure and a cost-effective manner for PKA activity assays, and shows great potential in clinical diagnosis and drug discoveries.

1. Introduction

Protein phosphorylation regulated by protein kinase and protein phosphatase is important posttranslational modification mechanism and plays cardinal roles in many fundamental cellular processes in eukaryotes, such as signal transduction, cell cycle and transcription (Hunter, 1994). The degree of protein phosphorylation at a certain site depends on the activity of the cognate protein kinase or phosphatase or both (Hunter, 1995). Thus, abnormal protein phosphorylation and aberrant protein kinase activities are closely coupled with many diseases, such as some neurodegenerative diseases, cancers and diabetes (Beristain et al., 2015; Chen et al., 2012; Myeku et al., 2016; Wang et al., 2013). Protein kinase inhibitors can down-regulate the activities of relevant protein kinase and have been emerged as promising drugs for treatment of a series of diseases (Marin et al., 2012; Weickhardt et al., 2012). Therefore, accurate identification of protein kinase activity and their potential inhibitors evaluation are not only essential for the kinase-targeted diagnosis, therapies and drug discoveries, but also helpful for clarifying the molecular signal transduction pathways. Thus, rapid and sensitive assays for protein kinase activity detection and kinase inhibitors screening are highly desirable.

Up to now, various approaches for the protein activity detection have been developed, the traditional one is radiometric methods that use radioactive ^{32}P-labeling (Hastie et al., 2006). However, the inherent drawbacks such as harmful radioactive labels and sophisticated instrumentation limit its further applications. Therefore, alternative techniques have been developed, such as fluorescence (Bai et al., 2013; Shen et al., 2015; Song et al., 2015), chemiluminescence (Wang et al., 2015; Zhao et al., 2015a), mass spectrometry (Deng et al., 2014), and electrochemistry (Shin et al., 2014; Wang et al., 2011), etc. Among these methods above,

* Corresponding authors.
E-mail addresses: zonghuawang@qdu.edu.cn (Z. Wang), jbcai@ustc.edu.cn (J. Cai), liu-yang@mail.tsinghua.edu.cn (Y. Liu).

http://dx.doi.org/10.1016/j.bios.2017.05.011
Received 20 February 2017; Received in revised form 27 April 2017; Accepted 4 May 2017
Available online 05 May 2017
0956-5663/

photoelectrochemical (PEC) approach has aroused special attention due to its high sensitivity and hence better analytical performance (Chen et al., 2010; Tang et al., 2013; Wu et al., 2015; Zang et al., 2015; Zhao et al., 2015b, 2014). In the PEC platform, light is utilized to excite PEC active species and the generated photocurrent is utilized as detection signal. Benefiting from the separation of excitation source and detection signal, the PEC method is very sensitive. What's more, it exhibits other merits over the traditional techniques, such as easy readout, inexpensive devices and simple operation (Zhang et al., 2013). Recently, a few of PEC biosensors have been designed for the detection of kinase activity. For example, PEC biosensors for protein kinase A activity determination have been reported based on the specific recognition ability of biotinylated Phos-tag for kinase-induced phosphopeptides combined with the inhibition of electron transfer of streptavidin tag (Zhou et al., 2015) or signal improvement of alkaline phosphatase (Yin et al., 2015). In addition, a sensitive PEC sensing platform for T4 polynucleotide kinase detection based on gold nanoparticles-decorated g-C_3N_4 nanosheets was developed, and DNAzyme-mediated catalytic precipitation signal amplification strategy was applied to improve the sensitivity (Zhuang et al., 2015). However, despite of the improvement of these methods, the synthesizing process of the photoactive species is usually strict and complicated, and generally biotag labeling is needed. Besides, to improve the performances of the PEC sensors, some of the photoactive species are used, such as quantum dots (QDs), noble metal nanoparticles etc. Even though they are effective, most of them are toxic and unstable. For instance, silver nanoparticles are easily oxidized during the light illumination. In addition, QDs have inherent drawbacks such as potential toxicity, high photo bleaching threshold, easy to hydrolysis and oxidation, which limit the applications of the PEC approaches (Zhang et al., 2014).

Metal-organic frameworks (MOFs) are a class of crystalline inorganic-organic hybrids, and they feature large surface area, flexible porosity, easily tailorable compositions and active sites. These remarkable advantages make MOFs attractive in gas storage/separation (Li et al., 2014), catalysis (Liu and Li, 2016), sensing (Zhan et al., 2013), as well as drug delivery (Qin et al., 2012; Tan et al., 2015). UiO series of Zr-cluster-based MOFs are integrated with the merits of high stability in aqueous conditions and less toxicity. Due to the high porosity, they can accommodate a large number of photoactive dye molecules, which can improve the light harvest efficiency. What's more, the metal centers in UiO series of MOFs can serve as “QDs”, together with the strong π-π stacking and Van Der Waals interaction between UiO series of MOFs and dye, the electron transport distance can be shorten in the electrode interface. As a result, the electron transfer rate and photo-to-current conversion efficiency can be largely improved (Yuan et al., 2015). In addition, Zr-O clusters in the UiO series of MOFs present high affinity toward phosphoric groups, and they can serve as anchorages for the recognition of phosphoric groups via the formation of Zr-O-P bonds. The high affinity toward phosphoric groups makes Zr-based MOFs being used in phosphates and phosphonates enrichment. For example, UiO-66 nanoparticles with exposed Zr-O clusters and ordered open cavities have been utilized for capture of alendronate, what's more, the Zr-based MOFs also have shown promise in specific enrichment and recognition of phosphopetides (Zhang et al., 2016; Zhu et al., 2015).

Inspired by this, a PEC biosensor for ultrasensitive protein kinase A (PKA) activity detection and inhibitor evaluation was fabricated by utilizing the Zr-cluster-based MOFs (UiO-66 as the model) as anchorages for phosphate groups and carriers for photoactive dyes. In this strategy, when the kemptide modified on TiO_2 fabricated ITO (TiO_2/ITO) electrode was phosphorylated in the presence of protein kinase A (PKA), $[Ru(bpy)_3]^{2+}$ loaded UiO-66 ($[Ru(bpy)_3]^{2+}$@UiO-66) probes were specifically chelated to the phosphorylated kemptide based on the high affinity between surface Zr^{4+} defects on Zr-O clusters and phosphate groups in phosphorylated kemptide. Under visible light irradiation, a sharp photocurrent produced and was applied for PKA activity detection. The simple and cost-effective fabricated PEC biosensor demonstrated good performances with a rapid response and high sensitivity. What's more, the kinase activities analysis in complicated cell lysates samples stimulated by ellagic acid and Forskolin were also carried out. This strategy affords a simple, sensitive and universal platform for kinase activity assays, and presents highly promise in kinases-related life science and medicament field.

2. Material and methods

2.1. Materials and reagents

Cysteine-terminated kemptide (CLRRASLG) was obtained from GL Biochem (Shanghai, China). PKA (catalytic subunit from bovine heart), Adenosin triphosphate (ATP) was obtained from Dingguo Biological Products Company (China). Tris(2,2′-bipyridyl) dichlororuthenium (II) hexahydrate ($Ru(bpy)_3Cl_2{\cdot}6H_2O$, $[Ru(bpy)_3]^{2+}$), Zirconium chloride ($ZrCl_4$), 1,4-benzenedicarboxylic acid (BDC), and N, N-Dimethylformamide (DMF) were purchased from Aladdin Chemistry Co., Ltd (Shanghai, China). 4,4′,5,5′,6,6′-hexahydroxydiphenic acid 2,6,2′,6′-dilactone (ellagic acid), N-(3-chlorophenyl)-6,7-dimethoxy-4-quinazolinamine (Tyrphostin AG1478), Forskolin and 3-isobutyl-1-methylxantine (IBMX) were purchased from Sigma. Other regents of analytical grade were provided by Beijing Chemical Company (China).

2.2. Apparatus and characterization

Photocurrent measurements were carried on a CHI802B electrochemical workstation (Chenhua Instrument Company of Shanghai, China) with 0.1 M PBS containing 0.1 M ascorbic acid (pH 7.4) as electrolyte. The electrochemical cell was in a typical three-electrode configuration: the modified electrode (working electrode), platinum wire counter electrode and Ag/AgCl, saturated KCl (reference electrode). Electrochemical impedance spectroscopy (EIS) was performed on the PARSTAT 2273 (Princeton Applied Research, USA). Ultraviolet-visible (UV–vis) spectra were measured on a UV-3900 spectrophotometer (Hitachi, Japan). Scanning electron microscope (SEM) images were obtained with a Hitachi SU8010 (Japan). Powder X-ray diffraction (XRD) patterns were conducted on a Bruker D8-Advance using Cu Kα radiation (λ=1.5418 Å). Fourier transform infrared spectroscopy (FT-IR) spectra was recorded on a QUINX55 spectrometer (Brucher, Germany). Scanning transmission electron microscopy (STEM), and energy-dispersive X-ray (EDX) elemental mapping images were all recorded on a JEM 2010 (120 kV) high-resolution transmission electron microscope.

2.3. Synthesis of UiO-66 nanoparticles and $[Ru(bpy)_3]^{2+}$@UiO-66 probes

UiO-66 was synthesized following a modified protocol reported before (Wu et al., 2013). Briefly, 240 mg of $ZrCl_4$, 4 mL CH_3COOH and 0.118 mL H_2O were first dissolved in 32 mL of DMF with stirring for 10 min. After that, 94.94 mg of BDC was added into the solution, following the ultrasonic treatment for 30 min in a Pyrex vial. Then, the homogeneous mixture was transferred into a 40 mL Teflon-lined stainless steel autoclave at 120 °C for 24 h. After cooling down to room temperature, the resultant white suspension of UiO-66 particles was collected by centrifugation and then washed with DMF. The ultimately UiO-66 samples were obtained by being activated in high dynamical vacuum at 450 °C for hours. Then the synthetic UiO-66 particles were characterized by SEM, TEM and XRD (Fig. S1), showing them homogeneously dispersed cubic shapes and a mean diameter of 60 nm.

$Ru(bpy)_3]^{2+}$@UiO-66 probes were obtained by adding $[Ru(bpy)_3]^{2+}$ solutions into 0.02g UiO-66 samples and being gently stirred for 36 h, then followed by centrifugation. UV–vis spectra (Fig. S2), STEM and EDX elemental mapping were used to characterize the $[Ru(bpy)_3]^{2+}$@UiO-66 probes. The quantity of $[Ru(bpy)_3]^{2+}$ in UiO-66 was calculated to be 6.5×10^{-6} mol g^{-1}, which was measured by Fluorescence spectra.

2.4. Biosensor fabrication

The amino-silane grafted TiO_2/ITO slices were fabricated as reported previously (Yan et al., 2015). In brief, 1.5 mg/mL TiO_2 suspensions were drop-coated on clean ITO slices and heated at 200 °C for 15 h. The amino-silane grafted TiO_2/ITO slices were gotten by being silanized in a 5 wt% acetone aqueous solution of 3-(amino-propyl triethoysilane) (APTES). Prior to immobilization of kemptide, the silanized ITO slices were immersed in glutaraldehyde solutions for 1 h and immersed into a PBS (10 mM, pH 7.4) solution containing 500 μM cysteine terminated kemptide for 12 h. After washing by PBS solution, the electrode was immersed in 1 mM 6-aminohexanoic acid solution for 30 min to block the electrode. A PKA-catalyzed phosphorylation reaction was performed by incubating the modified electrode in a PBS solution (50 mM Tris-HCl and 20 mM $MgCl_2$, pH 7.4) containing PKA and ATP at 37 °C. The phosphorylated peptide modified electrode was then incubated in the solution containing $[Ru(bpy)_3]^{2+}$@UiO-66 probes at room temperature. After that, the resulted electrode was thoroughly washed to remove the nonspecific $[Ru(bpy)_3]^{2+}$@UiO-66, and was ready for photocurrent characterization. For the PKA inhibition and cell lysates assays, the procedures were similar to the standard protocol described above, except that different desired concentrations of inhibitor or cell lysates were added in the PKA reaction mixture.

2.5. Preparation of MCF-7 cell lysates

MCF-7 cells were cultured in DMEM medium supplement at 37 °C under a humidified atmosphere containing 5% CO_2. After being starved for 4 h, MCF-7 cells were treated with adenylyl cyclase activator Forskolin and IBMX solutions and PKA inhibitor ellagic acid, with final concentration at 25 μM. Then the cultured cells were treated with lysis buffer for 5 min, and the cell lysates were clarified. Finally, the resulting supernatants were stored at −80 °C and were ready for PKA activity and inhibition detection. The concentration of total protein of cultured cells calculated by Nanodrop were 28.891 mg/mL for Forskolin stimulated cells, 25.414 mg/mL for control cells and 24.072 mg/mL for ellagic acid stimulated cells, respectively.

3. Results and discussion

3.1. Protein kinase activity evaluation

Scheme 1 describes the principle of the PEC biosensor for the detection of PKA activity. The cysteine-terminated kemptide was firstly assembled on the TiO_2/ITO electrode through the reaction between aldehyde group of the glutaraldehyde and the amino group on the kemptide. Then, the modified electrode was treated with 6-aminohexanoic acid as blocking reagent to avoid non-specific adsorption. In the presence of PKA, the kemptide was phosphorylated and chelated to $[Ru(bpy)_3]^{2+}$@UiO-66 probes by forming Zr-O-P bonds between Zr-O clusters in UiO-66 and phosphate groups in phosphorylated kemptide. $[Ru(bpy)_3]^{2+}$@UiO-66 modified on the electrode could harvest visible light to produce excited electrons. The conduction band of UiO-66 is estimated to be −0.6 V vs NHE, meanwhile, the LUMO potential of $[Ru(bpy)_3]^{2+}$ is −1.24 V vs NHE (Kim et al., 2014), thus excited electrons could transfer though UiO-66 and inject into the TiO_2 conduction band to form the photocurrent. The photo-to-current conversion efficiency of the PEC platform was further improved due to the strong π-π stacking and Van Der Waals interaction between $[Ru(bpy)_3]^{2+}$ and UiO-66 (Khlobystov et al., 2001). Therefore, the as-designed PEC biosensor provides a sensitive tool for kinase activity evaluation.

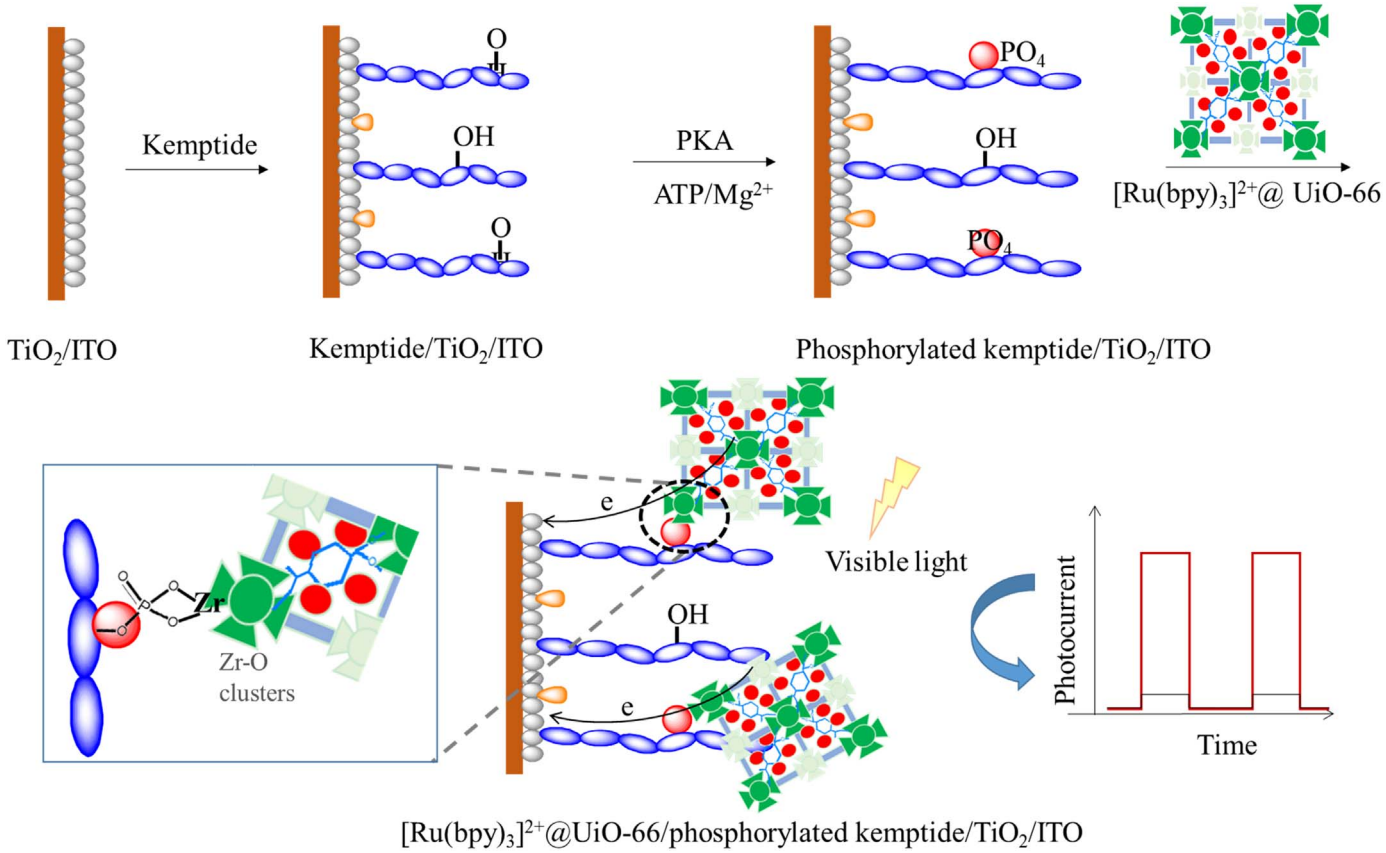

Scheme 1. The configuration of PEC biosensor for kinase activity detection.

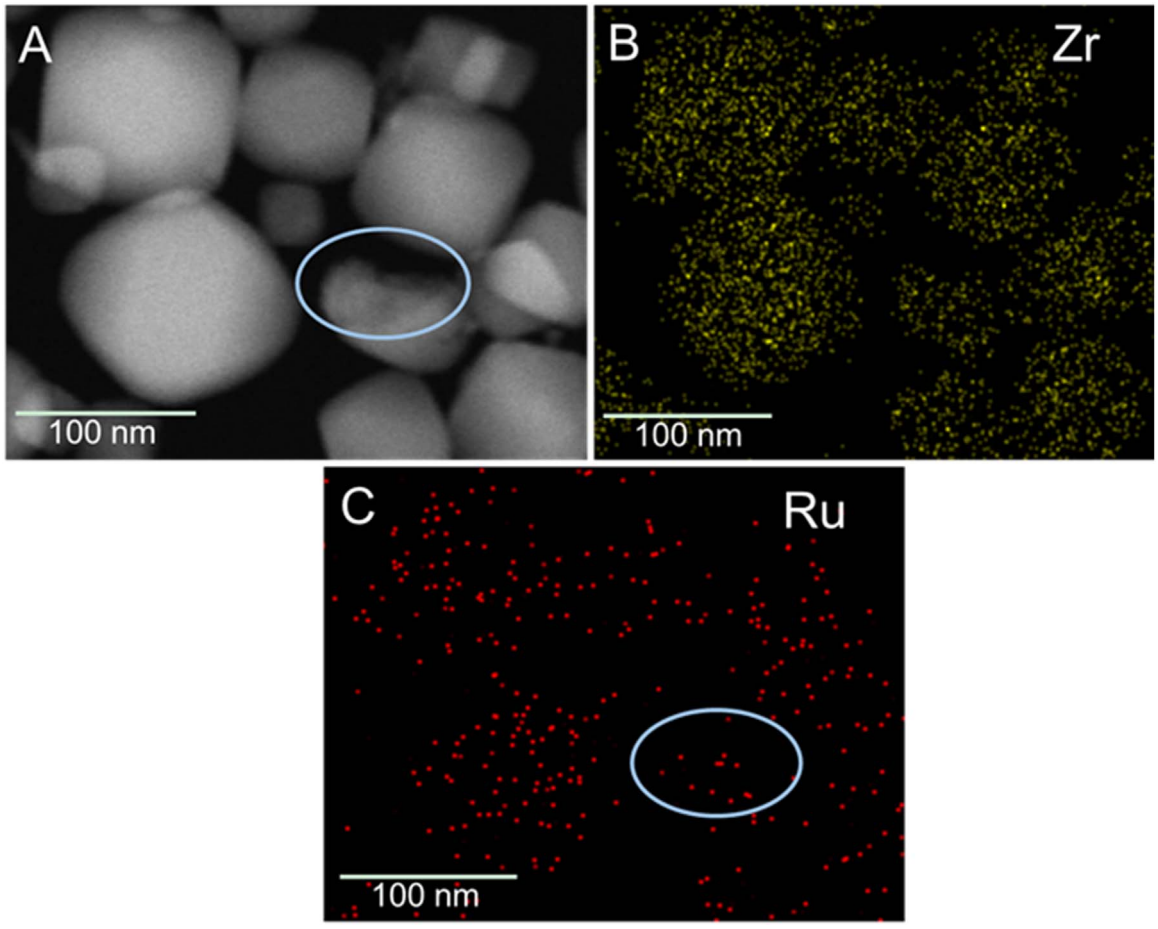

Fig. 1. SEM image and EDX elemental mapping of Zr and Ru in $[Ru(bpy)_3]^{2+}$@UiO-66 probes.

3.2. Characterization of the $[Ru(bpy)_3]^{2+}$@UiO-66 probes and kemptide modified TiO_2/ITO electrode

The $[Ru(bpy)_3]^{2+}$@UiO-66 probes were confirmed by UV–vis spectra, SEM and EDX elemental mapping. Fig. 1A and Fig. S1C show the isolated $[Ru(bpy)_3]^{2+}$@UiO-66 crystal with cubical morphology. We further made EDX elemental mapping for Zr and Ru elements of $[Ru(bpy)_3]^{2+}$@UiO-66, which confirmed the homogenous distribution of Zr and Ru around UiO-66 (Fig. 1B, C). What's more, the EDX mapping image of Ru elements in the cross section of the broken $[Ru(bpy)_3]^{2+}$@UiO-66 indicated that $[Ru(bpy)_3]^{2+}$ dyes were absorbed in UiO-66 pores.

EIS was applied to characterize the modification processes of the electrode using $[Fe(CN)_6]^{4-/3-}$ as electroactive probes. The spectra were recorded in $[Fe(CN)_6]^{4-/3-}$ solution in the frequency range from 0.1 Hz to 100 kHz. As shown in Fig. 2A, the bare ITO electrode exhibited small electron-transfer resistance (R_{et}) value (curve a), attributing to a fast electron-transfer process. After the modification of TiO_2 and immobilization of the kemptide, the R_{et} of the electrode increased gradually (curve b and curve c). The fact could be attributed to the electron inert effect of kemptide and TiO_2, which blocks the transfer of electron on the electrode interface. After phosphorylated by PKA (curve d), the diameter of semicircle successively increased, suggesting the decrease of electron transfer rate on the electrode interface. The fact could be ascribed to the replacement of hydroxide group by phosphate group that increased the negative charge density of kemptide, and hence hindered the electron transfer at the electrode interface. Finally, when treated with $[Ru(bpy)_3]^{2+}$@UiO-66 probes, the modification of UiO-66 obstructed electron-transfer on the electrode interface, thus the Ret increased (curve e).

The phosphorylation of kemptide and surface defect recognition of UiO-66 were confirmed by FT-IR spectra. As it is shown in Fig. 2B, besides the characteristic peaks of kemptide, additional peaks at 923 cm^{-1} was appeared and it was attributed to the phosphate groups catalyzed by PKA (Ji et al., 2009). When UiO-66 probes were modified on the phosphorylated kemptide, the phosphate group peak was shifted to 960 cm^{-1}, which was ascribing to the Zr-O-P bonds (Zhu et al., 2014). There are about one out of twelve missing linker defects in UiO-66, in which the positive charges on the metal centers would be balanced by terminal group (such as -OH groups) at the vacancy sites (Wu et al., 2013). These missing linker surface defects induced Zr-OH groups very reactive and could complex with phosphor bearing peptide to form Zr-O-P bonds. The Zr contraction led to closer packing of tetrahedral PO_4 groups and shorten P-O distance, thus yielded higher stretching and bending frequencies significantly (Begun et al., 1981).

3.3. PEC behaviors of the biosensor

The PEC behaviors of the modified electrode were studied. Fig. 3A presents the photocurrent responses of the modified electrode in 0.1 M PBS containing 0.1 M ascorbic acid under visible light irradiation. It was observed that both the ITO and TiO_2/ITO electrodes exhibited negligible photocurrent response under visible light. After treated with kemptide, and then phosphorylated by PKA, similar results were obtained. However, when $[Ru(bpy)_3]^{2+}$@UiO-66 was assembled on the phosphorylated kemptide modified electrode, sharply increased photocurrent was observed. This could be explained that when irradiated by visible light, $[Ru(bpy)_3]^{2+}$ molecules absorbed visible light and produced excited electrons, due to the short charge transport length as well as the strong π-π stacking and Van Der Waals interaction between $[Ru(bpy)_3]^{2+}$ and UiO-66, the excited electrons injected into the electrode efficiently and formed the photocurrent.

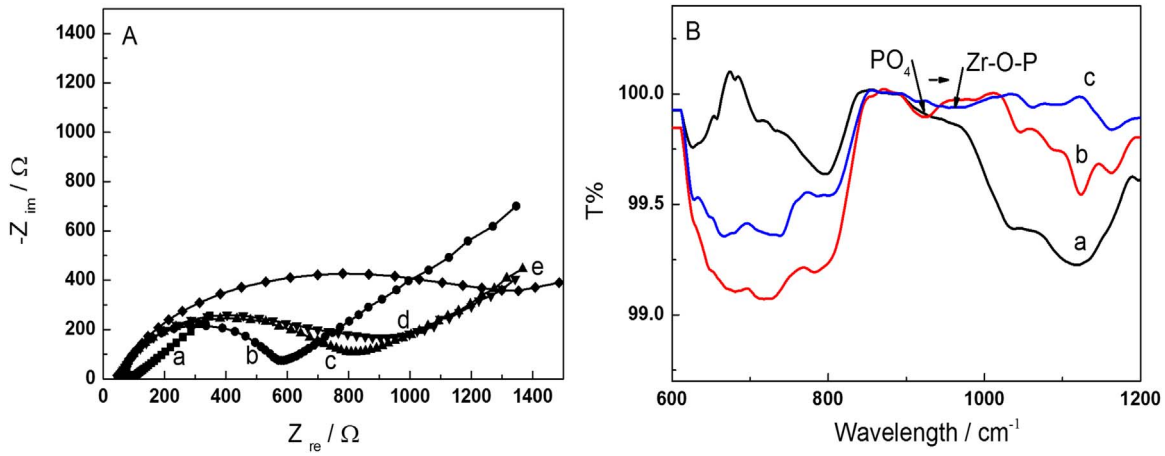

Fig. 2. (A) Electrochemical impedance spectra of (a) the bare ITO electrode, (b) TiO_2/ITO, (c) kemptide/TiO_2/ITO, (d) phosphorylated kemptide/TiO_2/ITO, (e) $[Ru(bpy)_3]^{2+}$@UiO-66/phosphorylated kemptide/TiO_2/ITO. The spectra were recorded in 0.1 M KCl solution with 5 mM $[Fe(CN)_6]^{3-/4-}$ electroactive probes. Scan rate is 100 mV/s. The frequency range is between 0.1 Hz and 100 kHz. (B) FT-IR spectra of kemptide modified electrode before (a), after (b) PKA treatment and (c) UiO-66 modification in the presence of ATP.

To testify the feasibility of the proposed design, a series control experiences were conducted. Fig. 3B shows the photocurrent responses on the phosphorylated kemptide (curve a) and kemptide (curve b) with the treatment of $[Ru(bpy)_3]^{2+}$@UiO-66. The kemptide/TiO_2/ITO electrode treated with $[Ru(bpy)_3]^{2+}$@UiO-66 presented a very weak photocurrent signal compared with the phosphorylated kemptide/TiO_2/ITO electrode. This was because in the absence of PKA, the kemptide couldn't be phosphorylated and hence failed to capture $[Ru(bpy)_3]^{2+}$@UiO-66 probes. After phosphorylated by kinase in the presence of ATP, strong photocurrent was collected due to the modification of $[Ru(bpy)_3]^{2+}$@UiO-66. When the phosphorylated kemptide modified electrode was merely treated with UiO-66, negligible photocurrent was observed compared with the $[Ru(bpy)_3]^{2+}$@UiO-66 modified electrode, demonstrated the meliority of the $[Ru(bpy)_3]^{2+}$@UiO-66 probes for PKA activity analysis and inhibition evaluation.

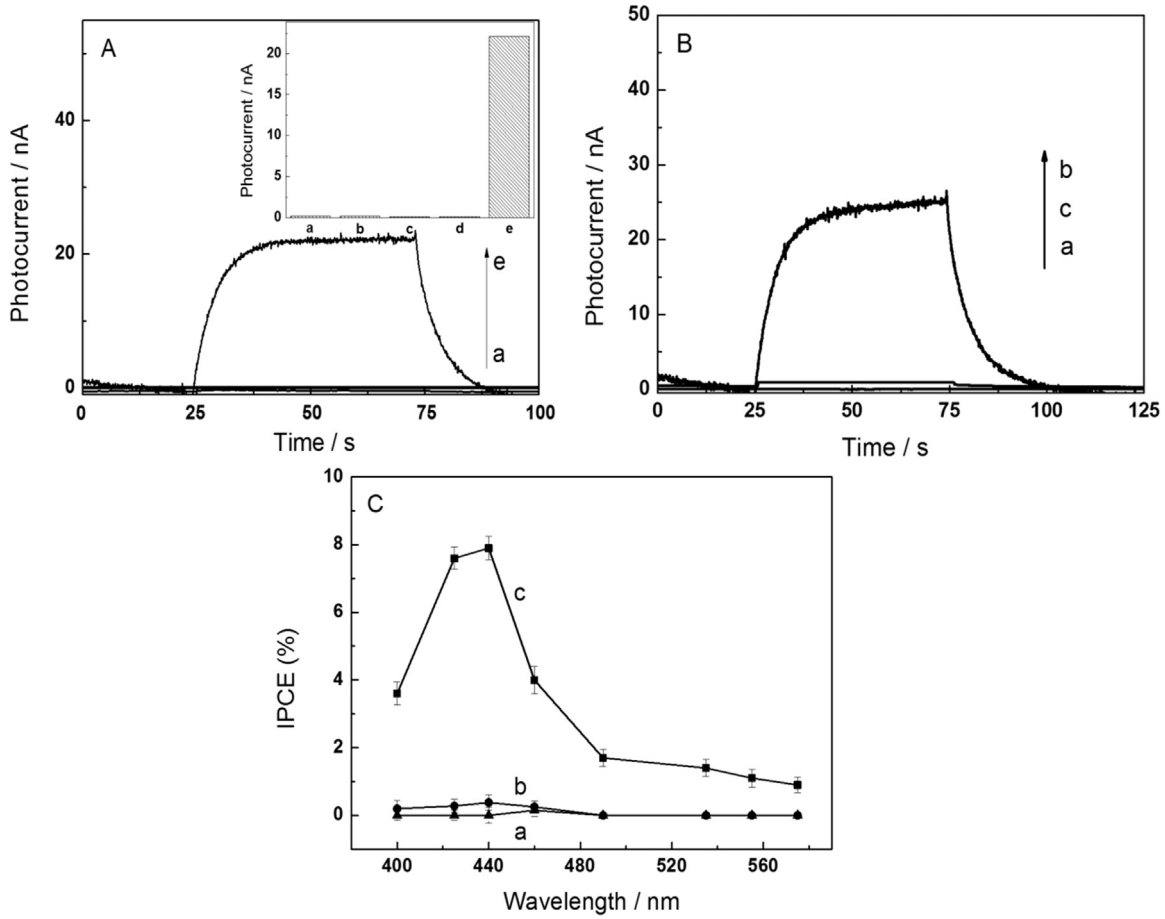

Fig. 3. The photocurrent behaviors of the biosensors. (A) The transient photocurrent responses of (a) the bare ITO electrode, (b) TiO_2/ITO, (c) kemptide/TiO_2/ITO, (d) PKA catalyzed phosphorylated kemptide/TiO_2/ITO, (e) $[Ru(bpy)_3]^{2+}$@UiO-66/phosphorylated kemptide/TiO_2/ITO. (B) The photocurrent response of (a) $[Ru(bpy)_3]^{2+}$@UiO-66/ kemptide/TiO_2/ITO, (b) $[Ru(bpy)_3]^{2+}$@UiO-66/phosphorylated kemptide/TiO_2/ITO, (c) UiO-66/phosphorylated kemptide/TiO_2/ITO. (C) Dependence of IPCE spectra on (a) UiO-66/TiO_2/ITO electrodes, (b) $[Ru(bpy)_3]^{2+}$/TiO_2/ITO electrodes and (c) $[Ru(bpy)_3]^{2+}$@UiO-66/TiO_2/ITO electrodes from 400 nm to 575 nm. The light power density is 190 mW cm^{-2}, electrode area is 0.5 cm^2.

The photocurrent of the modified electrode in the photocurrent action spectra from 400 nm to 575 nm was collected with a xenon lamp light source equipped with bandpass filters, The incident photon to photocurrent efficiency (IPCE) for each wavelength (λ) was calculated according to the Equation below:

$$IPCE = [(1240/\lambda) \times (J_{light} - J_{dark})/P_{light}] \times 100\% \quad (1)$$

Where J_{light}, J_{dark} are the respective current densities in the dark and light and P_{light} is the light power density (Li et al., 2013).

Fig. 3C shows IPCE plots for the electrodes conjugated with $[Ru(bpy)_3]^{2+}$@UiO-66, UiO-66 and $[Ru(bpy)_3]^{2+}$ respectively. It was clearly that the IPCE value of $[Ru(bpy)_3]^{2+}$@UiO-66 modified electrode was much higher than the IPCE value of UiO-66 modified electrode and $[Ru(bpy)_3]^{2+}$ modified electrode, indicated higher efficiency of the photon to electron conversion for $[Ru(bpy)_3]^{2+}$@UiO-66 probes. Accordingly, the as-proposed strategy could be used for sensitive PKA activity analysis.

3.4. Optimization of the detection conditions

ATP acts cofactor and offers the phosphate groups during the phosphorylation reaction. Therefore, its concentration was optimized in our experiments. As shown in Fig. S3A in the supporting information, the photocurrent increased with the increasing of ATP concentration and reached a plateau at 80 μM. Thus, 80 μM ATP was chosen in the PKA activity study. The phosphorylation time has also been assayed. From Fig. S3B, with the increasing phosphorylation time, the photocurrent signal increased accordingly and reached a maximum level at 80 min. Therefore, 80 min for phosphorylation has been employed in further experiments. In addition, the time for $[Ru(bpy)_3]^{2+}$@UiO-66 probes incubating on the phosphorylated kemptide was also investigated. The optimal time was 60 min in these experiments (Fig. S3C).

3.5. PEC measurements of PKA activity

The assessment of PKA activities was carried out under the optimized experimental conditions. Fig. 4 shows the changes of the photocurrent as a function of PKA activity. The photocurrent intensities increased with increasing activity of PKA and then reached a platform value after 20 U mL^{-1}. As shown in the inset of Fig. 3, the photocurrent was proportional to the PKA activity in the range from 0.005 U mL^{-1} to 0.0625 U mL^{-1} with a correlation equation of I =− 0.559+296c, where I was the photocurrent intensity and c was the kinase activity. The corresponding detection limit for PKA was estimated to be 0.0049 U mL^{-1} (S/N =3), which showed obviously excellent performance compared with the previous reported assays

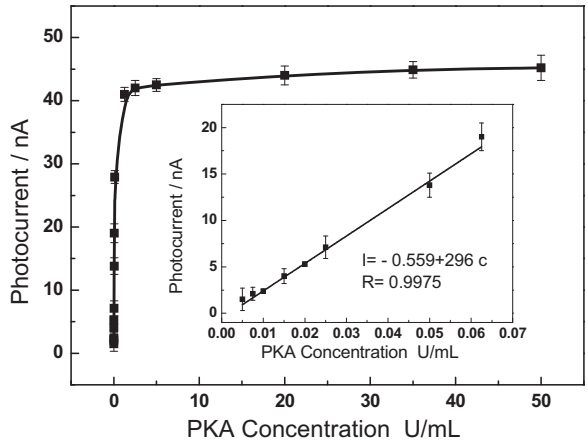

Fig. 4. The photocurrent intensities at different PKA concentrations from 0.005 U mL^{-1} to 50 U mL^{-1}. The inset is the linear relationship between current intensities and PKA concentrations. The light power density is 190 mW cm^{-2}, electrode area is 0.5 cm^2.

(Sun et al., 2015; Yang et al., 2015). The repeatability of the proposed method was evaluated by detecting assaying the same level of PKA activity of 1 U mL^{-1} using 6 independently fabricated biosensors. The relative standard deviation for ten determinations was 6.87%, indicating acceptable detection repeatability. Stability of the designed biosensor was also evaluated by assaying the PKA activity of 0.05 U mL^{-1} and the RSD was 4.33%, indicating the good stability of the biosensor. The facts demonstrate that the proposed PEC method can be applied for PKA activity detection with high sensitivity.

3.6. Inhibition evaluation and PKA activity detection in cell lysates

To demonstrate the potential application in the inhibition assay, the kinase activities were measured under a fixed PKA concentration with different concentrations of kinase inhibitors. As shown in Fig. 5A, with increasing concentrations of ellagic acid, a cell-permeable inhibitor of PKA, the photocurrent intensity decreased and then reached a stable level when the concentrations of ellagic acid were over 10 μM. The reason was that the PKA activity was inhibited when treated with ellagic acid, thus resulted low levels of kemptide phosphorylation. The half-maximal inhibition values (IC50) was calculated to be 4.21 μM, which was comparable with our previous result (Liu et al., 2014). In addition, the PKA activity analysis was also conducted in the presence of Tyrphostin AG 1478, which is a tyrosine kinase inhibitor but not a PKA inhibitor. As seen in curve b of Fig. 5A, the photocurrent signal had negligible change with the concentration change of Tyrphostin AG 1478, indicating the non-influenced effect. These results indicate that the as-designed PEC biosensor is potential in quantitative kinase inhibitors screening.

PKA plays crucial roles in cellular activities, abnormal expression caused by extracellular stimulation can generate a series of cellular problems. Herein, the activation and inhibition of the intracellular PKA from MCF-7 cells with the treatment of Forskolin combined with IBMX and ellagic acid respectively were measured by the PEC biosensor. As shown in Fig. 5B, it was observed that the MCF-7 cells treated with ellagic acid exhibited lowest PKA activity while the cell lysate treated with Forskolin exhibited the highest level of PKA activity among these samples. The fact could be attributed to the addition of Forskolin along with IBMX, which increased the intracellular levels of cAMP, caused the activation of PKA, and thus resulted high levels of kemptide phosphorylation. What's more, MCF-7 cells were stimulated with different concentrations of Forskolin and IBMX and the corresponding PKA activities in cell lysates were evaluated (Fig. 5C). The photocurrent intensities increased with the increasing concentrations of Forskolin and IBMX, indicating an enhanced PKA activity. Therefore, the change of PKA activity in cells stimulated by extracellular drugs can be detected via this PEC platform, indicating its potential in vitro cell kinase assays.

4. Conclusions

In conclusion, a novel sensitive turn-on PEC biosensor using UiO-66 as anchorages for phosphate groups and multiple photocurrent signal amplification has been developed for kinase activity and inhibition assay. $[Ru(bpy)_3]^{2+}$@UiO-66 probes were chelated to phosphorylated kemptide by forming Zr-O-P bonds between the Zr^{4+} defects in UiO-66 and phosphate groups in phosphorylated kemptide. The excited electrons generated by the $[Ru(bpy)_3]^{2+}$ under visible light irradiation transferred to electrode to form the photocurrent, meanwhile, the photo-to-current efficiency of the PEC system was highly improved by UiO-66, for it can facilitate the charge separation and transportation. A sensitive detection limit of 0.0049 U mL^{-1} was obtained, what's more, the as-designed PEC biosensor has also successfully been applied in quantitative kinase inhibitor screening and PKA activities detection in stimulated cell lysates. Therefore, the present work provides a promising technique for drug discovery applications and kinase related signal transduction pathways.

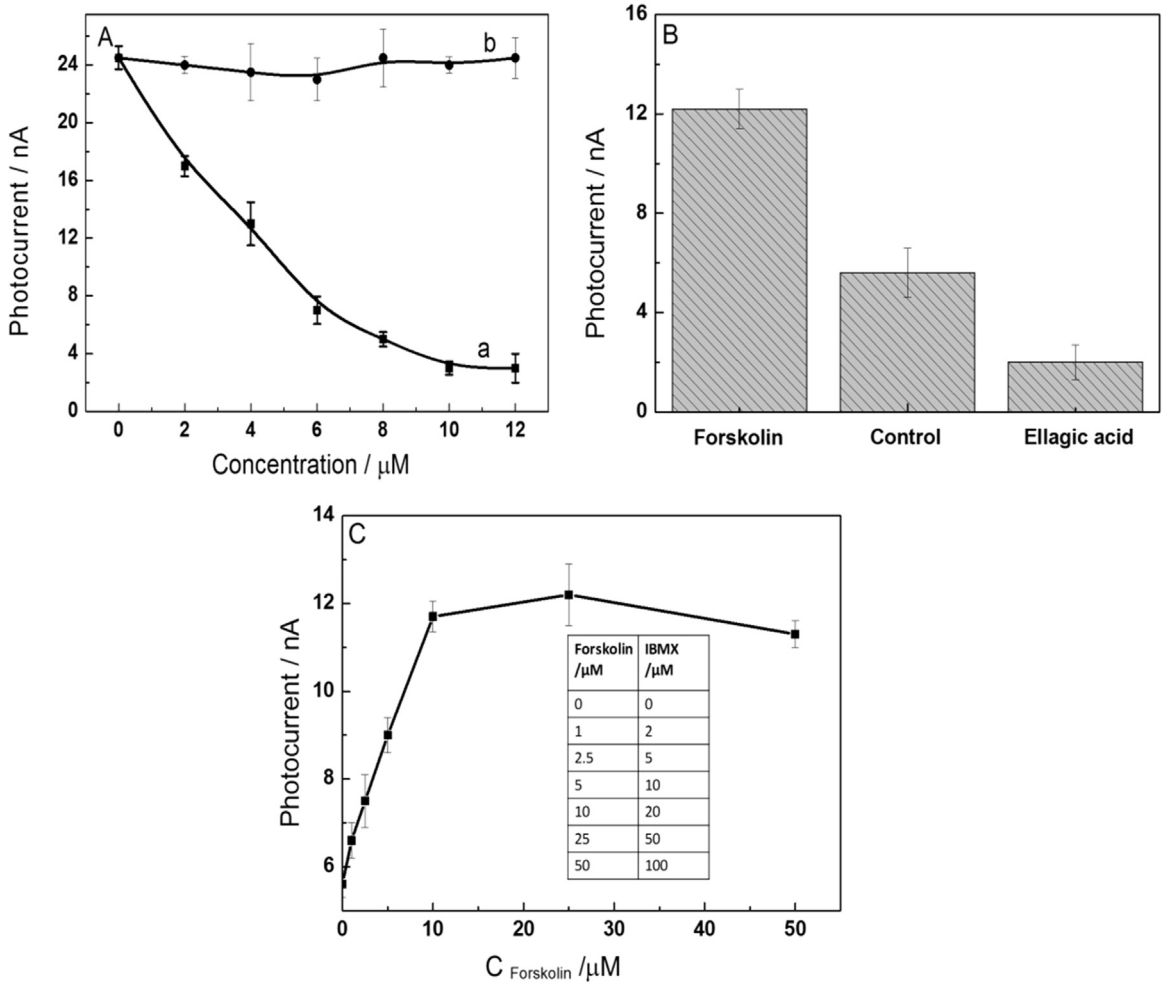

Fig. 5. (A) The photocurrent responses of different concentrations of ellagic acid (a) and Tyrphostin AG 1478 (b). The concentrations of PKA and ATP are 0.1 U mL^{-1} and 100 μM, respectively. (B) The PKA expression of MCF-7 cells treated with Forskolin and ellagic acid. (C) The dependence of the photocurrent on different concentrations of Forskolin and IBMX. The light power density is 190 mW cm^{-2}, the electrode area is 0.5 cm^2.

Acknowledgments

This work was financially supported by National Key Research and Development Program of China (No. 2016YFA0203101), National Basic Research Program of China (No. 2013CB934004), National Natural Science Foundation of China (Nos. 21622506, 21375073, 21235004, 21621003, 21405086, 21475071 and 21275082), and Tsinghua University Initiative Scientific Research Program (2014z21027), Beijing Municipal Science And Technology Commission (Z171100001117135), the Taishan Scholar Program of Shandong Province (No. ts201511027).

Appendix A. Supplementary material

Supplementary data associated with this article can be found in the online version at doi:10.1016/j.bios.2017.05.011.

References

Bai, J., Zhao, Y.J., Wang, Z.B., Liu, C.H., Wang, Y.C., Li, Z.P., 2013. Anal. Chem. 85, 4813–4821.
Begun, G., Beall, G., Boatner, L., Gregor, W., 1981. J. Raman Spectrosc. 11, 273–278.
Beristain, A., Molyneux, S., Joshi, P., Pomroy, N., Di Grappa, M., Chang, M., Kirschner, L.S., Privé, G., Pujana, M., Khokha, R., 2015. Oncogene 34, 1160–1173.
Chen, D., Zhang, H., Li, X., Li, J.H., 2010. Anal. Chem. 82, 2253–2261.
Chen, Y.M., Huang, X.M., Zhang, Y.W., Rockenstein, E., Bu, G.J., Golde, T.E., Masliah, E., Xu, H.X., 2012. J. Neurosci. 32, 11390–11395.
Deng, Z.Z., Ye, M.L., Bian, Y.Y., Liu, Z.Y., Liu, F.J., Wang, C.L., Qin, H.Q., Zou, H.F., 2014. Chem. Commun. 50, 13960–13962.
Hastie, C.J., McLauchlan, H.J., Cohen, P., 2006. Nat. Protoc. 1, 968–971.
Hunter, T., 1994. Semin. Cell Biol. 5, 367–376.
Hunter, T., 1995. Cell 80, 225–236.
Ji, J., Yang, H., Liu, Y., Chen, H., Kong, J.L., Liu, B.H., 2009. Chem. Commun., 1508–1510.
Khlobystov, A.N., Blake, A.J., Champness, N.R., Lemenovskii, D.A., Majouga, A.G., Zyk, N.V., Schröder, M., 2001. Coord. Chem. Rev. 222, 155–192.
Kim, J.H., Lee, M., Park, C.B., 2014. Angew. Chem., Int. Ed. 53, 6364–6368.
Li, B., Wen, H.M., Zhou, W., Chen, B.L., 2014. J. Phys. Chem. Lett. 5, 3468–3479.
Li, Y., Zhang, L., Torres-Pardo, A., Gonzalez-Calbet, J.M., Ma, Y., Oleynikov, P., Terasaki, O., Asahina, S., Shima, M., Cha, D., Zhao, L., Takanabe, K., Kubota, J., Domen, K., 2013. Nat. Commun. 4, 2566.
Liu, C.H., Chang, L.J., Wang, H.H., Bai, J., Ren, W., Li, Z.P., 2014. Anal. Chem. 86, 6095–6102.
Liu, M.J., Li, J.H., 2016. ACS Appl. Mater. Interfaces 8, 2158–2165.
Marin, D., Ibrahim, A.R., Lucas, C., Gerrard, G., Wang, L.H., Szydlo, R.M., Clark, R.E., Apperley, J.F., Milojkovic, D., Bua, M., 2012. J. Clin. Oncol. 30, 232–238.
Myeku, N., Clelland, C.L., Emrani, S., Kukushkin, N.V., Yu, W.H., Goldberg, A.L., Duff, K.E., 2016. Nat. Med. 22, 46–53.
Qin, J.S., Du, D.Y., Li, W.L., Zhang, J.P., Li, S.L., Su, Z.M., Wang, X.L., Xu, Q., Shao, K.Z., Lan, Y.Q., 2012. Chem. Sci. 3, 2114–2118.
Shen, C.C., Xia, X.D., Hu, S.Q., Yang, M.H., Wang, J.X., 2015. Anal. Chem. 87, 693–698.
Shin, I.S., Chand, R., Lee, S.W., Rhee, H.W., Kim, Y.S., Hong, J.I., 2014. Anal. Chem. 86, 10992–10995.
Song, W., Liang, R.P., Wang, Y., Zhang, L., Qiu, J.D., 2015. Chem. Commun. 51, 10006–10009.
Sun, S.J., Shen, H.X., Liu, C.H., Li, Z.P., 2015. Analyst 140, 5685–5691.
Tan, L.L., Li, H.W., Zhou, Y., Zhang, Y.Y., Feng, X., Wang, B., Yang, Y.W., 2015. Small 11, (3806-3806).
Tang, J., Kong, B., Wang, Y.C., Xu, M., Wang, Y.L., Wu, H., Zheng, G.F., 2013. Nano Lett. 13, 5350–5354.
Wang, D.J., Luo, P., Wang, Y.B., Li, W.J., Wang, C., Sun, D.D., Zhang, R.Q., Su, T., Ma, X.W., Zeng, C., 2013. Diabetes 62, 1697–1708.
Wang, J., Cao, Y., Li, Y., Liang, Z.Q., Li, G.X., 2011. J. Electroanal. Chem. 656, 274–278.
Wang, Z.H., Yan, Z.Y., Sun, N., Liu, Y., 2015. Biosens. Bioelectron. 68, 771–776.
Weickhardt, A.J., Scheier, B., Burke, J.M., Gan, G., Lu, X., Bunn, P.A., Aisner, D.L.,

Gaspar, L.E., Kavanagh, B.D., Doebele, R.C., 2012. J. Thorac. Oncol. 7, 1807–1814.
Wu, H., Chua, Y.S., Krungleviciute, V., Tyagi, M., Chen, P., Yildirim, T., Zhou, W., 2013. J. Am. Chem. Soc. 135, 10525–10532.
Wu, P., Pan, J.B., Li, X.L., Hou, X.D., Xu, J.J., Chen, H.Y., 2015. Chem. – Eur. J. 21, 5129–5135.
Yan, Z.Y., Wang, Z.H., Miao, Z., Liu, Y., 2015. Anal. Chem. 88, 922–929.
Yang, W.X., Lu, X.H., Wang, Y.C., Sun, S.J., Liu, C.H., Li, Z.P., 2015. Sens. Actuators B 210, 508–512.
Yin, H.S., Sun, B., Dong, L.F., Li, B.C., Zhou, Y.L., Ai, S.Y., 2015. Biosens. Bioelectron. 64, 462–468.
Yuan, Y.P., Yin, L.S., Cao, S.W., Xu, G.S., Li, C.H., Xue, C., 2015. Appl. Catal. B 168, 572–576.
Zang, Y., Lei, J.P., Ling, P.H., Ju, H.X., 2015. Anal. Chem. 87, 5430–5436.
Zhan, W.W., Kuang, Q., Zhou, J.Z., Kong, X.J., Xie, Z.X., Zheng, L.S., 2013. J. Am. Chem. Soc. 135, 1926–1933.
Zhang, G.Y., Cai, C., Cosnier, S., Zeng, H.B., Zhang, X.J., Shan, D., 2016. Nanoscale 8, 11649–11657.
Zhang, X.Q., Zhang, X.Y., Tao, L., Chi, Z.G., Xu, J.R., Wei, Y., 2014. J. Mater. Chem. B. 2, 4398–4414.
Zhang, X.R., Guo, Y.S., Liu, M.S., Zhang, S.S., 2013. RSC Adv. 3, 2846–2857.
Zhao, H.F., Liang, R.P., Wang, J.W., Qiu, J.D., 2015a. Chem. Commun. 51, 12669–12672.
Zhao, M., Fan, G.C., Chen, J.J., Shi, J.J., Zhu, J.J., 2015b. Anal. Chem. 87, 12340–12347.
Zhao, W.W., Xu, J.J., Chen, H.Y., 2014. Chem. Rev. 114, 7421–7441.
Zhou, Y.L., Wang, M., Yang, Z.Q., Yin, H.S., Ai, S.Y., 2015. Sens. Actuators B 206, 728–734.
Zhu, X.Y., Gu, J.L., Wang, Y., Li, B., Li, Y.S., Zhao, W.R., Shi, J.L., 2014. Chem. Commun. 50, 8779–8782.
Zhu, X.Y., Gu, J.L., Yang, J., Wang, Z., Li, Y.S., Zhao, L.M., Zhao, W.R., Shi, J.L., 2015. J. Mater. Chem. B 3, 4242–4248.
Zhuang, J.Y., Lai, W.Q., Xu, M.D., Zhou, Q., Tang, D.P., 2015. ACS Appl. Mater. Interfaces 7, 8330–8338.